A connectivity-constrained computational account of topographic organization in primate high-level visual cortex

Nicholas M. Blauch $^{a,b,\mp}$, Marlene Behrmann $^{b,c,\mp}$, and David C. Plaut b,c

^a Program in Neural Computation, Carnegie Mellon University; ^b Neuroscience Institute, Carnegie Mellon University; ^c Department of Psychology, Carnegie Mellon University
This manuscript was compiled on June 21, 2022

Inferotemporal cortex (IT) in humans and other primates is topographically organized, containing multiple hierarchically-organized areas selective for particular domains, such as faces and scenes. This organization is commonly viewed in terms of evolved domainspecific visual mechanisms. Here, we develop an alternative, domain-general and developmental account of IT cortical organization. The account is instantiated in Interactive Topographic Networks (ITNs), a class of computational models in which a hierarchy of model IT areas, subject to biologically-plausible connectivity-based constraints, learns high-level visual representations optimized for multiple domains. We find that minimizing a wiring cost on spatially organized feedforward and lateral connections alongside realistic constraints on the sign of neuronal connectivity within model IT results in a hierarchical, topographic organization. This organization replicates a number of key properties of primate IT cortex, including the presence of domain-selective spatial clusters preferentially involved in the representation of faces, objects, and scenes, columnar responses across separate excitatory and inhibitory units, and generic spatial organization whereby the response correlation of pairs of units falls off with their distance. We thus argue that topographic domain-selectivity is an emergent property of a visual system optimized to maximize behavioral performance under generic connectivity-based constraints.

13

14

15

21

 $\label{thm:continuous} Inferotemporal cortex \mid Functional organization \mid Topography \mid Neural network \mid Development$

nferotemporal cortex (IT) subserves higher-order visual abil-• ities in primates, including the visual recognition of objects and faces. By adulthood in humans, IT cortex, and ventral temporal cortex more generally, contains substantial functional topographic organization, including the presence of domain-selective spatial clusters in reliable spatial locations, including clusters for faces (1-3), objects (4), buildings and scenes (5, 6), and words (7). Similar domain-level topographic properties have been found in rhesus macaque monkeys, including multiple regions of clustered face selectivity (8–10). Intriguingly, this selectivity is encompassed in a larger scale "mosaic" of category-selectivity, in which areas of categoryselectivity themselves have further columnar clustering within them (11–13), and moreover, category-selectivity appears to exist as clusters within general dimensions of object space (14) spatially organized so as to smoothly map neuronal correlations over space (15), pointing to more general principles of organization beyond the domain level. In line with this idea, human IT cortex also exhibits larger-scale organization for properties such as animacy and real-world size (16, 17), and midlevel features characteristic of these properties and domains have been shown to account well for patterns of highlevel visual selectivity (18). How these domain-level and more

general facets of functional organization arise, how they are related, and whether and in what ways they rely on innate specification and/or experience-based developmental processes remain contentious.

25

26

28

29

30

31

35

36

37

38

41

42

43

44

Recent work has demonstrated that the neural basis of face recognition depends crucially on experience, given that deprivation of face viewing in juvenile macaque monkeys prevents the emergence of face-selective regions (19). Relatedly, the absence of exposure to written forms through reading acquisition precludes the emergence of word-selective regions (20, 21). That there exists clustered neural response selectivity for evolutionarily new visual categories such as written words offers further evidence that the topographic development of the human visual system has a critical experience-dependent component (22, 23). In contrast with a system in which innate mechanisms are determined through natural selection, this experiential plasticity permits the tuning of the visual system based on the most frequent and important visual stimuli that are actually encountered, thereby enabling greater flexibility for ongoing adaptation across the lifespan.

There is considerable computational evidence that experience-dependent neural plasticity can account for the response properties of the visual system at the single neuron level. Classic work demonstrated that the statistics of natural images are sufficient for learning V1-like localized edge-tuning

Significance Statement

We introduce the Interactive Topographic Network, a framework for modeling cortical organization of high-level vision. We demonstrate in computational simulations that the spatial clustering of domains in late stages of the primate visual system may arise from the demands of visual recognition under the constraints of minimal wiring costs and biologically realistic constraints on the sign of neuronal connections. The learned organization of the model is highly specialized but not fully modular, capturing many of the properties of organization in primates. Our work is significant for cognitive neuroscience, by providing a domain-general developmental account of topographic functional specialization, and for computational neuroscience, by demonstrating how well-known biological details can be successfully incorporated into neural network models in order to account for critical empirical findings.

N.M.B., M.B., and D.C.P. conceived of the work. N.M.B. developed software and performed simulations and data analyses. M.B. and D.C.P supervised the project. N.M.B. wrote the first draft of the paper. N.M.B, M.B., and D.C.P. revised the paper.

The authors declare no competing interests.

 $[\]mp$ To whom correspondence should be addressed. E-mail: {blauch,behrmann}@cmu.edu

within a sparse coding framework (24, 25). More recently, deep convolutional neural networks (DCNNs) trained on image classification have been successful in accounting for the tuning of neurons in V1, V2, V4, and IT in a hierarchically consistent manner, where deeper layers of the DCNN map onto later layers of the anatomical hierarchy (26, 27).

50

51

52

54

55

56

57

58

59

60

61

63

64

65

66

67

71

72

73

74

75

76

77

78

79

80

81

82

83

84

85

86

87

88

89

90

91

92

93

94

95

96

97

98

101

102

103

104

105

107

109

Above the single-neuron level, considerable prior work has demonstrated that topographic organization in V1 may emerge from self-organizing, input-driven mechanisms (28–34) (for review, see 35). For example, the pinwheel architecture of spatially repeating smooth orientation selectivity overlaid with global retinotopy has been shown to be well-accounted for by Self-Organizing Maps (SOMs) (31, 32, 36).

One notable application of an SOM to modeling highlevel visual cortex by Cowell and Cottrell (37) demonstrated stronger topographic clustering for faces compared to other object categories (e.g., chairs, shoes), suggesting that the greater topographic clustering of faces in IT is due to greater withincategory similarity among faces compared to these other categories. This work provides a strong case for domain-general developmental principles underlying cortical topography in IT, but at least two important issues remain unaddressed. First, rather than only supporting discrimination of face from nonface categories (as in 37), face representations in humans (and likely non-human primates, though see (38)) must support the more difficult and fine-grained task of individuation; this task requires a "spreading transformation" of representations for different face identities (39, 40), which could could alter the feature space and its topographic mapping, and necessitate a more domain-specialized representation than that examined by (37). Second, rather than a single face-selective area, IT cortex actually contains multiple hierarchically-organized face-selective regions with preferential inter-connectivity (41). Generally, SOMs are not well equipped to explain such hierarchical topographic interactions, as they are designed to map a feature space into a topographic embedding, but not to transform the feature space hierarchically in the way needed to untangle invariant visual object representation from the statistics of natural images (42). This suggests that SOMs are an incomplete model of topographic development in cortical networks.

An alternative approach to studying topographic organization involves incorporating distance-dependent constraints on neural computation within more general neural network models (43–46). Of particular interest is a hierarchical neural network developed by Jacobs and Jordan (45) in which error-driven learning was augmented with a spatial loss function penalizing large weights to a greater degree on longer versus shorter connections. This model was shown to develop topographic organization for 'what' versus 'where' information when trained with spatially segregated output units for the two tasks. Closely related work by Plaut and Behrmann (47) demonstrated that a similarly spatially-constrained model with biased demands on input (e.g., retinotopy) and output (e.g. left-lateralized language) could account for the organization of domain-specific areas in IT cortex, such as the foveal bias for words and faces, leftward lateralization of words, and rightward lateralization of faces (48–50).

However, to date, none of these structurally-biased neural network models have been applied to large-scale sets of naturalistic images, the statistics of which are thought to organize high-level visual representations in IT cortex (51), and the topography in these models (45, 47) has been analyzed at a relatively coarse level. Nonetheless, this early work raises the possibility that the application of distance-dependent constraints in a deep neural architecture trained on natural images might provide a more comprehensive account of topographic organization in IT.

110

111

112

113

114

115

116

117

118

119

120

121

122

123

124

125

126

127

130

131

132

133

134

135

137

138

139

140

141

142

144

145

146

147

148

149

150

151

152

153

154

155

156

157

158

159

160

161

162

164

165

166

167

168

169

170

171

Along these lines, Lee and colleagues (15) have recently modeled the topography of IT cortex with Topographic Deep Artificial Neural Networks (TDANNs) that are trained on a large set of natural images using a correlation-based layout that explicitly encourages units within a layer of the network to be spatially nearer to units with correlated responses, and farther from units with uncorrelated or anti-correlated responses. As a result, the TDANN developed face-selective topography that corresponded well with data from macaque monkeys. However, this approach *imposes* topographic functional organization on the network based on measured functional responses, rather than deriving it from realistic principles of cortical structure and function, such as constraints on connectivity. Moreover, like the SOM, the TDANN can explain only within-area topographic organization, and not spatial relationships between areas, such as stream-like organization of multiple stages of IT cortex (3, 52) and their embedding in a network coupled with upstream and downstream cortical areas (48). Thus, the question remains whether such basic structural principles can account for the topographic organization of IT.

In the current work, we combined the approaches of taskoptimized DCNN modeling (15, 51) with flexible connectivityconstrained architectures (45, 47) to develop a hierarchical model of topographic organization in IT cortex. We implemented a bias towards local connectivity through minimization of an explicit wiring cost function (45) alongside a task performance cost function. Intriguingly, we observed that this pressure on local connectivity was, on its own, insufficient to drive substantial topographic organization in our model. This led us to explore two neurobiological constraints on the sign of connectivity—strictly excitatory feedforward connectivity, and the separation of excitation and inhibition—with the result that both, and, particularly, excitatory feedforward connectivity, provided a powerful further inductive bias for developing topographic organization when combined with a bias towards local connectivity. Our results begin to shed light on the factors underlying hierarchical topographic organization in the primate visual system.

Materials and Methods

The Interactive Topographic Network. We introduce the Interactive Topographic Network (ITN), a framework for computational modeling of high-level visual cortex, and specifically, it's functional topographic organization. ITN models are defined as neural network models that are 1) optimized to perform naturalistic tasks (following 53) and 2) connectivity-constrained in a biologically plausible manner so as to give rise to functional organization (extending previous work by 45, 47). In this work, we introduce a form of ITN that is divided into three components: an encoder that approximates early visual cortex, interactive topography (IT) layers that approximate inferotemporal cortex, and a readout mechanism for one or more downstream tasks. The goal of the encoder is to extract general visual features which describe the visual world along dimensions that support a broad range of downstream readout tasks. However, our main modeling focus is on the IT layers, which consists of a series of pairs of recurrent layers that are subject to biological

constraints. For computational simplicity, such constraints are not modeled in the encoder (but see Discussion for future directions).

Encoder architecture and training. We used a ResNet-50 (54) encoder to allow the ITN to extract deep and predictive features of the trained inputs. The encoder is pre-trained on equal sized subsets of faces, objects, and scenes from the VGGFace2 (55), ImageNet (56), and Places365 (57) datasets, respectively, matched in terms of total training images. We reused the same subsets of faces and objects as in (58), and an additional scene domain was constructed to match the other two domains in total images. An initial learning rate of 0.01 was used, and this learning rate was decayed 5 times by a factor of 10 upon plateau of the validation error; after the fifth learning rate decay, the next validation error plateau determined the end of training. Stochastic gradient descent with momentum ($\rho = 0.9$) and l2 weight decay ($\lambda = 0.0001$) was used, with batch size of 256 on a single GPU.

Recurrent neural network formulation of IT. Our model of IT extends the standard discrete-time Recurrent Neural Network (RNN) formulation common in computational neuroscience (e.g., 59). We begin with the continuous-time dynamics of units in an RNN layer, where $\boldsymbol{x}^{(a)}$ is the vector of pre-activation activities in area a of IT, $\boldsymbol{r}^{(a)}$ is the vector of post-activation activities in area a, $\boldsymbol{b}^{(a)}$ is the vector of baseline activities in area a, τ is the scalar neuronal time constant, and $W^{(a,b)}$ is the matrix of weights from area a to area b:

$$\tau \frac{d \boldsymbol{x}_{t}^{(a)}}{d t} = -\boldsymbol{x}_{t}^{(a)} + W^{(a,a)} \boldsymbol{r}_{t}^{(a)} + W^{(a-1,a)} \boldsymbol{r}_{t}^{(a-1)} + \boldsymbol{b}^{(a)} \quad [1]$$

where the activation function $r_t^{(a)} = [x_t^{(a)}]_+$ is positive rectification, also called a Rectified Linear Unit (ReLU). Applying the Euler method to integrate this first-order ordinary differential equation, with time step size Δt , and substituting $\alpha = \frac{\Delta t}{\tau}$, yields the discrete time update:

$$\boldsymbol{x}_{t}^{(a)} = (1 - \alpha)\boldsymbol{x}_{t-1}^{(a)} + \alpha \left(W^{(a,a)}\boldsymbol{r}_{t-1}^{(a)} + W^{(a-1,a)}\boldsymbol{r}_{t-1}^{(a-1)} + \boldsymbol{b}^{(a)} \right)$$
[2]

When training models with separate excitatory and inhibitory units, we noted that training could be extremely unstable and typically required some mechanism for achieving stability. To this end, we adopted layer normalization (60), without the trainable scaling parameter that is sometimes used (see 60, for more details). We found layer normalization to be extremely effective in stabilizing models and encouraging well-distributed activations (Figure S38). Where $\mu(x)$ is the mean of x, and $\sigma(x)$ is the standard deviation of x, and b is the learned bias term (moved outside of the layer normalization), the layer-normalized activities are given as:

$$egin{aligned} oldsymbol{z_t} &= rac{oldsymbol{x_t} - \mu(oldsymbol{x_t})}{\sigma(oldsymbol{x_t})} + oldsymbol{b} \ oldsymbol{r_t'} &= [oldsymbol{z_t}]_+ \end{aligned}$$

Incorporating layer normalization into our update equation yields the final update equation:

$$\boldsymbol{x}_{t}^{(a)} = (1 - \alpha)\boldsymbol{z}_{t-1}^{(a)} + \alpha \left(W^{(a,a)} \boldsymbol{r}_{t-1}^{\prime(a)} + W^{(a-1,a)} \boldsymbol{r}_{t-1}^{\prime(a-1)} \right)$$
[3]

Extending the standard RNN framework with biological constraints. Here, we outline the major biological constraints implemented in this work.

Spatial organization. An essential aspect of an ITN model is that each IT layer has a spatial organization (see also (15)). We chose to model layers as square grids, with each layer of the hierarchy of equal size (typically, a grid size length of 32, corresponding to a layer of 1024 units). We normalize the coordinates to lie in the range [0,1]. Each unit thus has a unique (x,y) coordinate which will be used to determine the distance-dependent network topology. In general, the specific choices about map spatial arrangement are not critical to the predictions of the model, but they can potentially be manipulated in certain ways in the service of other theoretical goals.

Spatial connectivity costs. We impose distance-dependent constraints on connectivity through a cost on longer connections throughout training. This basic formulation of the loss was introduced by Jacobs and Jordan (45) as a way to induce spatially organized task specialization, and was shown to do so in a simple neural network model trained on small-scale tasks. To our knowledge, no other research has examined this loss in modern deep learning architectures trained on natural images. We use a simple modification of the original loss function, using the squared Euclidean distance $(\mathcal{D}_{i,j})^2 = ||r_i - r_j||_2^2$ (in place of $(\mathcal{D}_{i,j})^{10} = ||r_i - r_j||_{10}^{10}$ distance (45)). By using the squared distance, we penalize longer connections disproportionally compared to shorter connections. The spatial loss on connections between areas a and b, $\mathcal{L}_w^{(a,b)}$, is given by:

$$\mathcal{L}_{w}^{(a,b)} = \sum_{i,j} \frac{\left(\mathcal{D}_{ij}^{(a,b)}\right)^{2} \left(W_{ij}^{(a,b)}\right)^{2}}{1 + \left(W_{ij}^{(a,b)}\right)^{2}}$$
[4]

The total spatial loss is the sum of the area-to-area spatial losses $\mathcal{L}_w = \sum_{a,b} \mathcal{L}_w^{(a,b)}$, and is added to the task-based loss as $\mathcal{L} = \mathcal{L}_t + \lambda_w \mathcal{L}_w$, on which gradient descent is performed. Additionally, in contrast to (45), we choose a single λ_w parameter, rather than varying it throughout training. For each architectural variant, we chose the λ_w that maximized a metric of generic topographic organization $(T_g$, Equation 7)

Connection noise. To approximate axon-specific variability in instantaneous firing rate (61), we apply multiplicative noise on the individual connections between neurons that is uniform over distance and layers. In practice, we find that connection noise helps to regularize the activations in the network, encouraging a more distributed representation that aids the formation of topography across a range of models (see Figure S39 for evidence that it is not absolutely necessary). Noise is sampled independently from a Gaussian distribution $\mathcal N$ centered at 0 with variance σ^2 at each time step of each trial, and is squashed by a sigmoidal function $S(x) = \frac{2}{1+e^{-x}}$, ensuring that the sign of each weight is not changed and each magnitude does not change by more than 100%. Thus, the noisy weight matrix $W_n^{(a,b)}$ from area a to area b on a given trial and time step is:

$$W_n^{(a,b)} = S(\mathcal{N}(0,\sigma)) * W^{(a,b)}$$
 [5]

Sign-based restrictions on neuronal connectivity. Standard neural networks gloss over a key detail of neuronal morphology—that single neurons obey Dale's Law, whereby all of their outgoing connections are either excitatory or inhibitory (ignoring modulatory neurons and other special, rare cases) (59). We employ this principle within our framework by replacing the single sheet of unconstrained neurons with parallel sheets of excitatory (E) and inhibitory (I) neurons. The second sign-based restriction we implement is that between-area interactions are carried out predominantly by excitatory pyramidal neurons. Thus, we restrict between-area feedforward connectivity to originate from the excitatory neurons only. In the main model, both E and I neurons receive feedforward inputs.

IT architecture and training. The main ITN model consists of 3 IT layers (pIT, cIT, aIT) with separate E and I populations, and feedforward connections sent only by E units. To facilitate training many models with fewer computational demands, the model is trained using a fixed pre-trained ResNet-50 encoder on smaller subsets of faces, objects, and scenes. Specifically, we created image subsets equal to the size of the popular CIFAR-100 dataset but at higher image resolution, containing 100 categories each with 500 training images and 100 validation images, resized to 112x112 pixels. Thus, the combined dataset contained 300 categories with 150,000 training images and 30,000 validation images. The same learning rate schedule as used for training the encoder was used. Stochastic gradient descent with momentum $(\rho=0.9)$ was used, with batch size of 1024 on a single GPU. In the main model, we used spatial regularization with $\lambda_w=0.05$, without additional weight decay on IT connections.

IT model variants. To better understand the relative importance of different aspects of model design that contribute to the development of topographic organization, we examine a variety of IT model variants containing different subsets of implemented constraints (Figure 6). Some of these models do not use separate populations of E and I units, but still restrict feedforward connectivity to be excitatory. In this case, we simply restrict the feedforward weights to be positive, despite the same neuron having both positive and negative lateral connections. In another case, separate populations of E and I units are both allowed to send feedforward projections. In yet another variant, we remove learned lateral connections entirely. This model is trained for a single time step, and the only recurrent computation is that of a single pass of layer normalization. Lastly, we explore a range of spatial regularization strengths.

289

291

292

294

295

296

297

299

300

301

302

303

304

305

306

307

308

309 310

311

312

313

314

315

316

317

319

320

321

322

324

325

326

327

328

330

331

332

333

334

335

336

337

338

339

340

341

342

343

345

347

348

350

351

353

354

356

357

Analyses of trained models. After training, the responses in IT layers are probed to investigate emergent task specialization and its topographic organization. We use three main approaches.

Mass univariate analyses. The first analytic approach is the simple mass-univariate approach, in which each unit is analyzed separately for its mean response to each stimulus domain (objects, faces, scenes), using untrained validation images from the same categories used in training. In addition to computing the mean response to each domain, we compute selectivity, a ubiquitous metric used in neuroscience, to analyze how responsive a unit is to one domain compared to all others. We compare the responses of each domain versus the others using a two-tailed t-test, and given the test statistic t, the significance value p of the test, and the sign of the test statistic s = sign(t), we compute the selectivity as $-s \log(p)$.

Searchlight decoding analysis. The second analysis approach is the multivariate searchlight analysis commonly used in fMRI (62), in which a pool of units are selected in a (circular) spatial window around each unit, and the accuracy for discriminating between different categories (e.g., hammer vs. screw-driver) in each domain (e.g., objects) is computed using the activations of only that pool of units; the mean accuracy value is assigned to the center unit, and the process is repeated for all units.

Lesion analysis. To assess the causal role of certain units in the performance of specific tasks, we adopt a lesioning approach in which the activities of lesioned units are set to 0 at each time step. This effectively removes them from processing, allowing the network's dynamics to unfold independently of these units. The effect of a lesion is measured by computing the accuracy following the lesion and relating that to the baseline accuracy.

The first type of lesion we perform is a spatial or *focal* lesion in which a circular neighborhood of size $p \times p$ units is selected. where p is the fraction of units selected and n is the total number of units in the area where the lesion is performed. The lesion is centered on a unit $u_{i,j}$ either randomly or according to the peak of a specific metric such as selectivity. To lesion spatial neighborhoods corresponding to regions of high domain selectivity, we take the selectivity map, perform spatial smoothing, and select the unit u of peak smoothed selectivity.

The second type of lesion sorts units according to a given selectivity metric irrespective of their spatial location. In this analysis, the $p \times n$ most selective units are chosen for a given lesion. This is done separately for the selectivity of each domain, as in the focal lesions. When the topography is smooth and the regions approximately circular, the selectivity-ordered and focal lesions yield similar results. However, to the extent that the topography is not perfectly smooth or circular, the selectivity-ordered lesion may knock-out a more relevant set of units for a given task.

Distance-dependent response correlation. We calculate the correlations of the responses of all pairs of units as a function of distance between them. Response correlation is computed for a given time step over a large number of images, either from all domains, or from each domain separately.

Topographic organization summary statistics. We compute two metrics of topographic organization—one indexing generic organization and the other, domain-level organization. The domain-level topography statistic T_d is a measure of how much the alignment of domain-level selectivity vectors between pairs of units falls off with distance. For a given layer l, cell type c, and neuron i, let us consider a 3-D vector of selectivity values for each domain s_i . Using the dot product $s_i \cdot s_j$ between selectivity vectors of $m = \binom{p}{2}$ pairs of neurons (to allow for magnitude effects), standardized over all neuron pairs as $z(\cdot)$, and assuming l and c are held constant, the domain-topography statistic T_d is then given as:

$$T_d = \frac{1}{m} \sum_{i,j}^{p} \frac{z(s_i \cdot s_j)}{\mathcal{D}_{i,j}}$$
 [6]

359

361

362

363

364

365

367

369

370

371

372

373

374

376

377

378

379

380

381

382

383

384

385

386

387

388

389

391

392

393

394

396

397

399

400

402

404

408

409

410

411

412

The standardization ensures that the statistic is not inflated for poorly trained networks with uniformly high correlation values across unit pairs. Similarly, the generic topography statistic is a measure of how much pairwise response correlation falls off with distance. For a given layer l, cell type c, and neuron i, let us consider a n-D vector of responses over n images s_i . The statistic T_g is then

$$T_g = \frac{1}{m} \sum_{i,j}^{p} \frac{z(r(a_i, a_j))}{\mathcal{D}_{i,j}}$$
 [7]

In the paper, we plot the T_g and T_d values averaged over layers and cell types. In supplementary material, we additionally plot values per layer and cell type.

Analyzing spatial costs of trained networks. To understand the wiring cost of certain trained models, we analyze the spatial cost of a network, as given by Equation 4, as a function of architectural parameters such as the spatial regularization strength λ_w . In one analysis, we analyze only the feedforward spatial cost, which simply requires summing spatial costs over pairs of areas a and b where $a \neq b$. Similarly, to analyze only the recurrent spatial cost, we can sum spatial cost over pairs of areas a and b where a = b.

Unweighted spatial cost of sparsified networks. While wiring cost in an artificial neural network should depend to some extent on the strength of connections—stronger connections may require greater myelination, and strong connections in an artificial neural network may correspond to a larger number of synapses in a biological neural network—there is another notion of wiring cost whereby it depends only on whether or not two neurons are connected. This notion of wiring costs has been commonly applied to the study of cortical areal layout and early visual cortical maps (e.g. 31, 63-65). Moreover, the analysis of binary connectivity in thresholded networks is also common in graph-theoretic analysis of brain data (66). To analyze this notion of wiring costs, we pruned our trained models to a desired connection sparsity level s, setting to 0 the $n \times m \times s$ connections with the smallest magnitude, where n and m are the number of units in areas a and b . Sparsity was enforced globally within IT and from IT to readout, rather than individually for each set of connections. We then analyzed an unweighted wiring $\cot \mathcal{L}_{w,u}^{(a,b)}$ that computes the mean of squared Euclidean distance values between connected units i and j in areas a and b, given that (a,b) are in the set of connected areas C:

$$\mathcal{L}_{w,u}^{(a,b)} = \frac{1}{n \, m \, (1-s)} \sum_{i,j} \left(\mathcal{D}_{ij}^{(a,b)} \right)^2 \left(W_{ij}^{(a,b)} \neq 0 \right)$$
 [8]

Results

A connectivity-constrained model of ventral temporal cortex produces hierarchical, domain-selective response topogra**phy.** We first present the results of simulations of a specific ITN model (Figure 1A), which we will refer to as the main model or E/I EFF RNN, to indicate that it possesses separate neurons responsible for excitation and inhibition (E/I), a restriction that feedforward connections are strictly excitatory (EFF), and temporally recurrent processing is mediated through learned lateral connections (RNN). These three factors—in addition to the strength of the wiring cost penalty λ_w —will be of interest

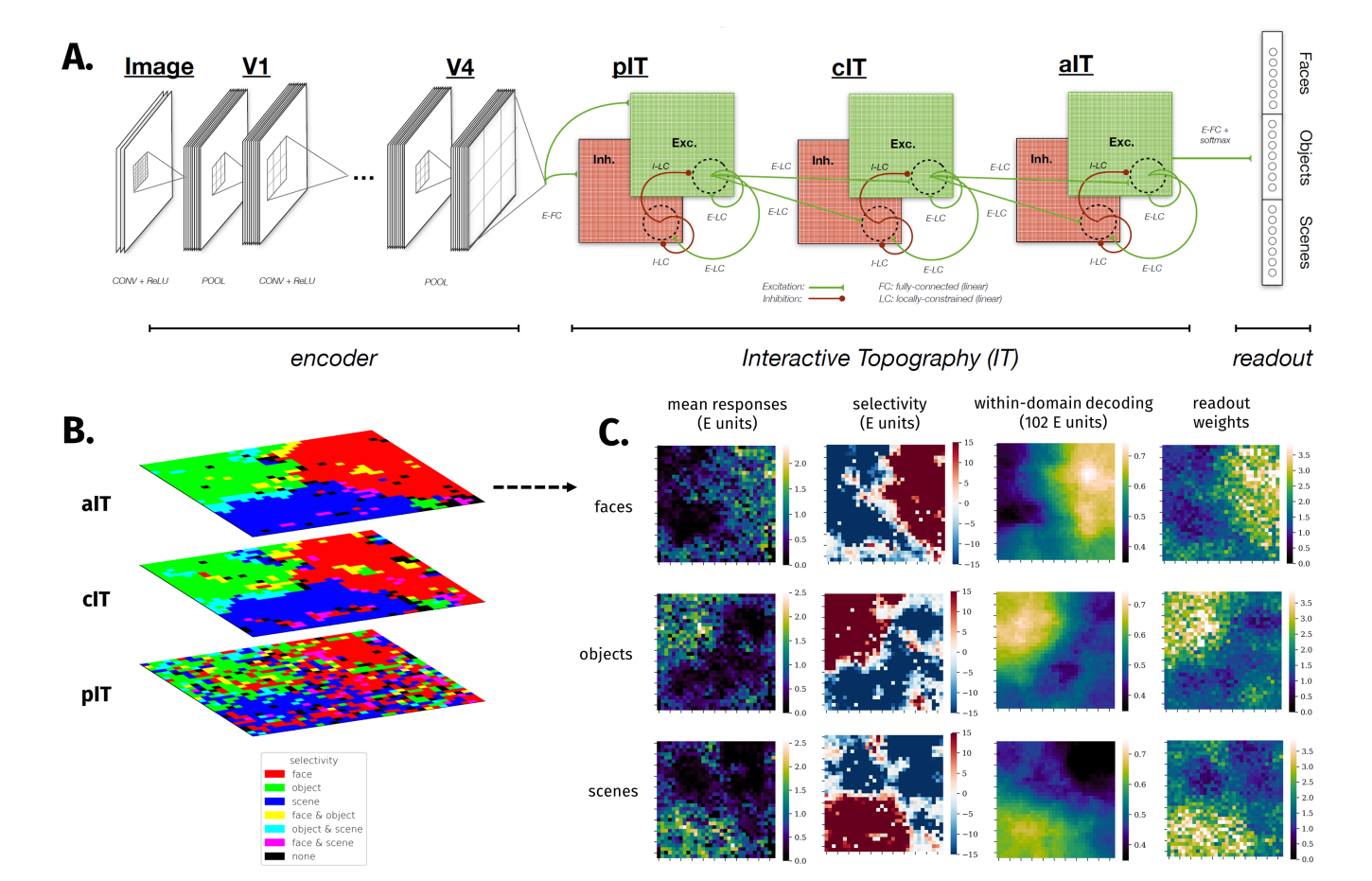


Fig. 1. The Interactive Topographic Network produces hierarchical domain-level organization. **A.** diagram of the Interactive Topographic Network (ITN). An ITN model consists of three components: an *encoder* that approximates early visual processing prior to inferotemporal cortex, the *interactive topography* (IT) areas that approximate inferotemporal cortex, and the *readout* mechanism for tasks such as object, scene, and face recognition. The architecture of each component is flexible. For example, a 4-layer simple convolutional network or a deep 50-layer ResNet can be used as the encoder; whereas the former facilitates end-to-end training along with a temporally-precise IT model, the latter supports better learning of the features that discriminate among trained categories. In this work, topographic organization is restricted to the IT layers. The figure depicts the main version of the ITN containing three constraints: a spatial connectivity cost pressuring local connectivity, separation of neurons with excitatory and inhibitory influences, and the restriction that all between-area connections are sent by the excitatory neurons. The final IT layer projects to the category readout layer containing one localist unit per learned category, here shown organized into three learned domains. (Note that this organization is merely visual and does not indicate any architectural segregation in the model. **B.** Domain selectivity at each level of the IT hierarchy. Selectivity is computed separately for each domain, and then binarized by including all units corresponding to p < 0.001. Each domain is assigned a color channel in order to plot all selectivities simultaneously. Note that a unit can have zero, one, or two selective domains, but not three, as indicated in the color legend. **C.** Detailed investigation of domain-level topography in aIT. Each heatmap plots a metric for each unit in aIT. The first column shows the mean domain response for each domain, the second column shows domain selectivity, the third column

later as we uncover the key ingredients of developing topography. Additionally, this model uses a ResNet-50 encoder which is pre-trained on a large dataset including several categories from the domains of objects, faces, and scenes (each domain matched in total training images), and following pre-training, is used as a feature extractor that provides input to a 3-area IT containing containing separate posterior (pIT), central (cIT), and anterior (aIT) areas. The main model used a spatial cost parameter $\lambda_w = 0.5$ which was chosen to maximize a metric of domain-level organization (Figure 6).

418

419

420

421

422

423

425

426

427

428

429

430

431

432

After training, the model performed well on each domain, reaching a classification accuracy of 86.4% on the face domain, 81.8% on the object domain, and 65.9% on the scene domain (see Figure S1). Performance differences across domains are unlikely to be an artifact of the specific architecture as they can be seen across a variety of DCNNs, reflecting the intrinsic difficulty of each task given the variability within and between

categories of each domain for the given image sets.

As can be seen in Figure 1B, the trained model exhibits domain-level topographic organization that is hierarchically linked across corresponding sectors of each layer. This result reflects the fact that the distance-dependent constraints on feedforward connectivity pressured units that have minimal between-area distances to learn a similar tuning, which means that each layer is roughly overlapping in their respective (separate) 2D topography. The topographic organization gets somewhat smoother moving from pIT to cIT, most likely because units in cIT and aIT (but not pIT) have local feedforward receptive fields and thus greater constraint on local cooperation. Further quantification of topographic organization in each layer can be found in Figure S6. Overall, the presence of domain-level topography—but not its particular spatial arrangement—was robust to variation elicited by random initialization of model parameters (Figure S23) (67).

435

436

437

438

439

440

442

443

444

445

446

447

448

449

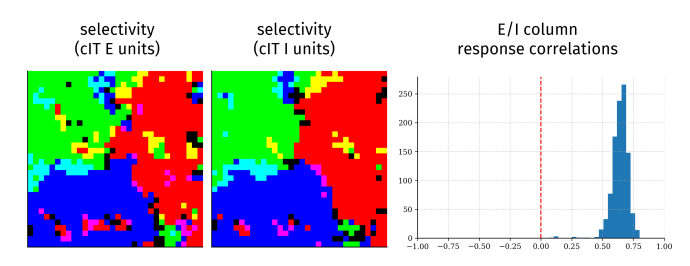


Fig. 2. E and I cells act as functional columns. Selectivity of cIT excitatory (E) units (left columns), and inhibitory (I) units (middle column) for each domain (colored as in Figure 1B), and histograms of response correlations between co-localized E and I units over all images.

We next scrutinized the topography in aIT, where there are very smooth domain-level responses, and where we can directly compare responses with those of the recognition readout mechanism. We computed mean domain responses, plotted in the first column of Figure 1C, and domain selectivity, plotted in the second column, which demonstrates corresponding topographic organization. We confirmed the functional significance of response topography by conducting a searchlight analysis inspired by multivariate approaches to analyzing functional magnetic resonance imaging (fMRI) data (62). used searchlights containing the 10% (102) nearest units. The results of this analysis, shown in the third column of Figure 1C, revealed topographic organization of information for discriminating between categories of each domain that is strongly correlated with the domain selectivity maps for each domain (all ps < 0.0001). Importantly, every searchlight contained information substantially above chance level for discriminating within each domain, pointing to partially distributed information despite topographic domain selectivity, in line with human and macaque neurophysiology (68, 69) (see Figure S3 for comparisons of searchlight decoding accuracy for each unit across domains).

To further confirm the functional significance of the topographic organization, we analyzed the spatial organization of readout weights from aIT to the localist category readout layer. We evaluated whether each domain placed more weight in reading out from the units for which there was greater selectivity, by calculating the mean domain response weight for each unit, averaged over classes in each domain. This produced a map for each domain, shown in the last column of Figure 1C. We find a large positive correlation between the mean readout weight and the mean response for each domain (all rs>0.7, all ps<0.0001), further demonstrating the functional significance of the response topography.

Excitatory and inhibitory units operate as functional columns.

In the main ITN model, the E cells serve as the principal neurons which exclusively project to downstream areas—thus, we have focused entirely on the E cells. The inhibitory (I) cells, in contrast, play a local role in processing, receiving inputs from and sending outputs to both E and I cells in the same cortical area. As all the neurons are subject to the same spatial constraint, we predicted that E and I neurons would have similar functional topographic organization. We show the topography of response selectivity of E and I neurons in area cIT in Figure 2. The neuron types demonstrate clearly similar functional topography, which we quantify at the columnar level of a pair of E and I units in the same location. We find

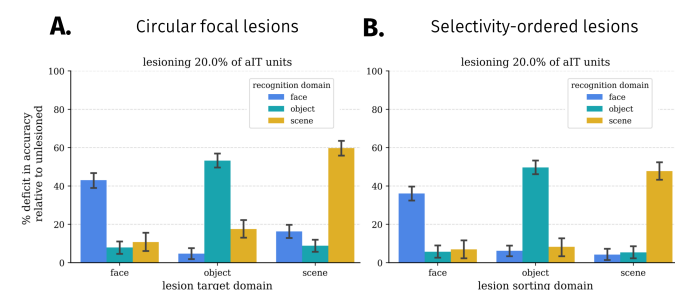


Fig. 3. Lesion results in the ITN model. Each plot shows the relative effects of a set of medium sized lesions (20% of alT units) on recognition performance for each domain, relative to the performance on the same domain in the undamaged model. Error bars show bootstrapped 95% confidence intervals over trials; thus, the statistical significance of a given lesion can be assessed by determining whether the confidence interval includes 0. **A.** Damage from circular focal lesions centered on the peak of smoothed selectivity for each domain. Left: results for a variety of lesion sizes. **B.** Damage from selectivity-ordered lesions for each domain.

that such E-I columns have highly correlated activity, implying specific functional coupling, as has been demonstrated in ferret visual cortex (70), and in cortical columns more generally (71). Inhibitory neurons in aIT yielded sparser selectivity and therefore weaker, but similar, coupling with E units (Figure S11). One reason I units in aIT may have sparser responses is that the network discovers that it can reduce inhibitory weights (and thereby spatial costs) here, as aIT units project onto readout units subject to a squashing softmax nonlinearity. E/I columnar organization was not found in a model trained without the spatial constraint (Figure S12).

Effects of lesions indicate strong yet graded domain-level specialization. We next performed a series of "lesion" analyses in the model in order to compare with neuropsychological data on face and object recognition (72–74). First, we performed focal lesions, as would be experienced by most patients with acquired brain damage. To simulate the impairment of patients with maximally specific deficits, we centered circular focal lesions of various sizes at the center of (smoothed) domain selectivity. Performance following each lesion was measured separately for each domain.

A subset of results of this lesion analysis using a medium sized lesion are shown in Figure 3A, with complete results in Figure S2. These focal lesions centered on each domain lead to an especially severe deficit in recognition for that domain, and milder but significant deficits for the other domains as well. For such lesions, the deficit is significant for all domains (all ps<0.05), and significantly stronger for recognition of the target domain (all ps<0.05).

Are these more general effects of circumscribed lesions on non-preferred domains the result of imperfect (patchy) or non-circular topographic organization of an underlying modular organization? To answer this question, we performed selectivity-ordered lesions, in which units were sorted by their selectivity for a given domain, and selected according to their sorting index. Again, a subset of results is shown in Figure 3B with complete results across a broader range of lesion sizes shown in Figure S2. The effects of damage in this case are similar to those for focal lesions, with greater damage to the domain on which sorting was performed, and smaller but significant deficits to other domains (all ps<0.05). This suggests that some but not all of the damage to the non-

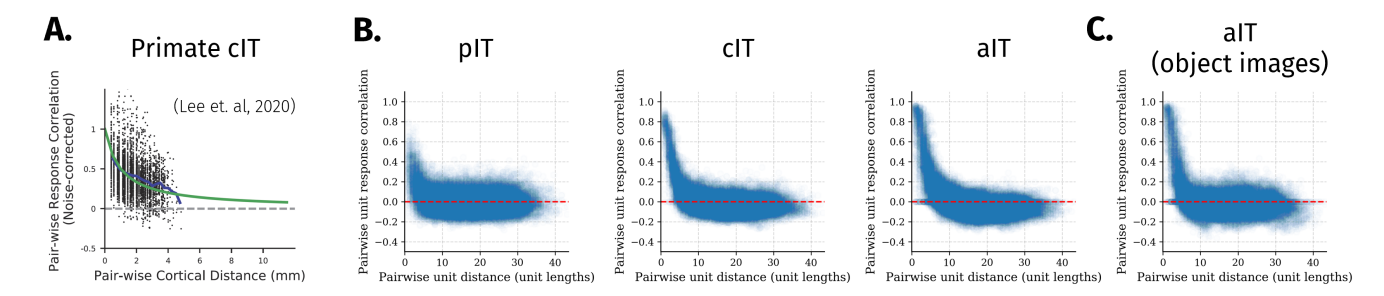


Fig. 4. Generic topographic organization beyond domain-selectivity emerges through task optimization under biologically-plausible constraints on connectivity. A. Distance-dependent response correlation in macaque IT (reproduced from 15, per CC-BY-NC-ND license). B. Distance-dependent response correlation in the excitatory cells of each layer, using images from all three domains (objects, faces, scenes). C. Distance-dependent response correlation in alT using images from the object domain only, highlighting within-domain generic functional organization.

preferred domain induced by focal lesions may be due to imperfect or non-circular topographic functional organization. Importantly, these more distributed effects of lesions indicate that the functional organization, while highly specialized, is not strictly modular; damage to those units purported to be a part of a given module (e.g. for face recognition) nevertheless affects object recognition (albeit to a weaker degree). Figures S3-S5 provide additional data on the nature of domain specialization in the network.

Domain selectivity exists within a broader organization similar to that of primate IT cortex. Previous empirical research has demonstrated that the response correlations between pairs of neurons fall off smoothly with increasing distance between the neurons (15, 75), as shown in Figure 4A. As discussed, this finding is the basis of TDANN models that explicitly fits the spatial layout of units to this relationship (15). We explored whether this relationship emerged naturally in our network due to its constrained connectivity, in line with the emergence of domain-selective topography. We thus computed the correlations among pairs of unit activations across images as a function of the distance between the units in each area. As shown in Figure 4B, there is, indeed, a smooth decay of response correlations with distance, matching the qualitative trend in the empirical data.

This result is not simply due to differences between domains, as it is also found when examining responses to images within each domain separately (shown for objects in Figure 4C). Along with previous results (15), our findings suggest that the domain-level topography may simply be a large-scale manifestation of a more general representational topography in which the information represented by neighboring units is more similar than that represented by more distal units. Our results demonstrate that this organization can arise under explicit wiring length and sign-based constraints on connectivity.

Generic organization encompasses interpretable domain-level and sub-domain level organization. Recently, Bao and colleagues (14) have provided evidence that IT cortex contains a map of object space that corresponds well to the first two principal components of high-level visual representations in an ImageNet-trained convolutional neural network, and that clusters in this object space corresponded to topographic clusters in IT cortex, including face-selective areas. We asked whether our network displayed a similar relationship. Similarly, we found that each domain lied in

weakly overlapping clusters of this PC1-PC2 space, where the first PC mostly separated faces and scenes, and the second PC separated objects from faces and scenes (Figure 5A, left). When we visualized the weights of these two PCs, we found that they were topographically organized (Figure 5B, right) and corresponded well to the large-scale domain structure inherent to aIT (see contour lines and Figure 1). Notably, relatively little within-domain clustering was seen along the first two PCs, and higher dimensions were less interpretable (Figure S20), and so, to seek finer-grained organization, we opted to visualize the principal components of activations to each domain separately, shown in Figure 5B. For each domain, we determined a within-domain attribute that might induce further representational—and thus, topographic—distinctions; we labeled whether the faces were male or female, whether objects were animate or inanimate, and whether scenes were indoors or outdoors. The PC1–PC2 space of each domain appeared to discriminate each attribute well but not necessarily exactly along either component, so we fit a logistic regression over the first two PCs to extract a line (2D hyperplane) in PC1-PC2 space that best discriminated between exemplars of each attribute type (i.e., $y(x) = w_1 \times PC_1(x) + w_2 \times PC_2(x)$); this led to discriminability of 0.84 for gender, 0.92 for animacy, and 0.87 for scenes. We then visualized the topographic weights from aIT onto these discriminating projections, revealing striking topographic organization. In each case, there was an ON-OFF weight pattern localized within the sector of domain-selectivity, along with further, weaker weight outside this sector—for example, orange-colored weight contributing to the animate object attribute within the face-selective cluster (Figure 5B, bottom center)—indicating graded contributions of non-selective units. A complementary clustering analysis of each domain yielded similar results, whereby categories with different attributes clustered spatially (Figures S8-S10).

Sign-based constraints combine with wiring length constraints to produce topographic organization. Having established that the main ITN architecture produces a host of empirically grounded topographic organizational phenomena, we next performed a constraint-removal analysis to determine which constraints—in addition to the bias towards local connectivity—are necessary for the development of topographic organization. We varied three binary constraints: whether between-area feedforward connections were excitatory only (EFF), whether the model employed separate E and I

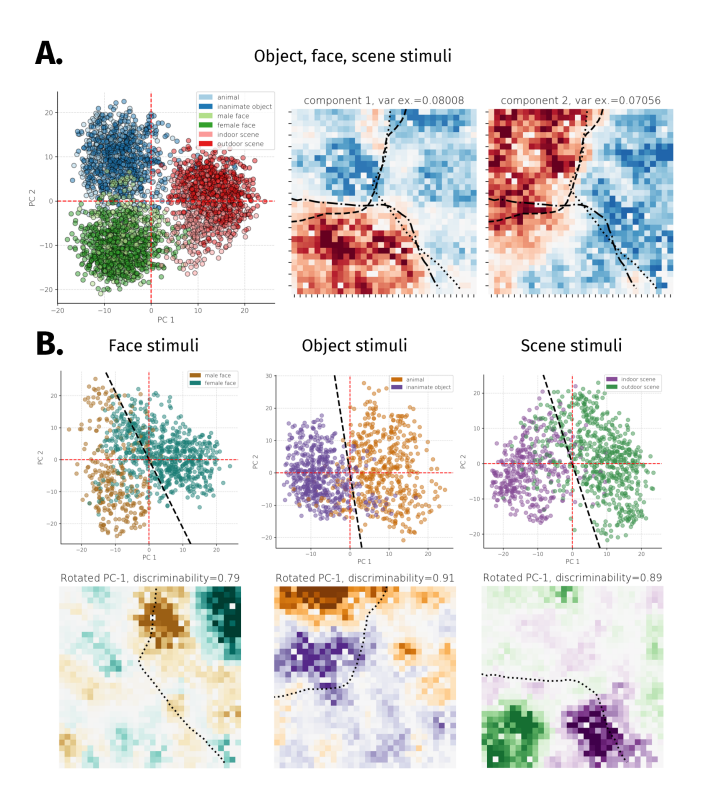


Fig. 5. Principal components analysis of activations. **A.** plots the PC1–PC2 space and PC1 and PC2 component weights across images from all three domains. Dashed lines on component weight plots show the contour of selectivity for each domain, using selectivity maps smoothed with a local averaging kernel (5% nearest units) corresponding to significance p<0.001. **B.** plots the PC1–PC2 space for responses to each domain separately, and the weight visualization of a rotated axis in PC1–PC2 space that maximized the discriminability of images according to a given sub-domain attribute (gender for faces, animacy for objects, and indoor/outdoor for scenes). Dashed lines show selectivity for the domain of interest, using selectivity maps smoothed with a local averaging kernel (5% nearest units) corresponding to significance p<0.001.

unit populations within each area (E/I), and whether the model contained lateral (recurrent) connections within each area (RNN vs. FNN). We thus constructed seven architectures (the I units in the E/I-EFF-FNN model would exert no effect, making the E/I-EFF-FNN model equivalent to the EFF-FNN model). Each of these architectures was trained across a log-spaced range of λ_w values, and the generic topography, domain-level topography, performance, and wiring cost were analyzed (Figure 6). For each architecture, we selected an optimal λ_w , chosen to maximize the measure of generic topography (Equation 7) averaged over layers and celltypes, trained an additional instance of the architecture with this λ_w , and visualized the learned topography, shown in Figure 6E. We found that models without sign constraints (RNN, FNN) produced only weak topography, uncharacteristic of primate IT cortex. In contrast, models with separate excitation and inhibition (E/I-RNN, E/I-FNN) produced somewhat greater topographic organization, and models with strictly excitatory feedforward connectivity (EFF-RNN, EFF-FNN) produced topographic organization equivalent to that of the main model (E/I-EFF-RNN). Moreover, temporal recurrence mediated through learned lateral connections was not necessary to develop topography. In terms of performance, we found that the accuracy of the various recurrent models was very similar, with a very small advantage for models in which feedforward connectivity was not constrained to be excitatory. In contrast, accuracy for the feedforward models was reduced more substantially (>4% points), pointing to a performance benefit of the recurrent connections. Moreover, while wiring cost (see next section) was determined much more by λ_w than architecture (Figure 6D), we found that, for the same λ_w across variants, the variants that developed clear domain-level organization had the smallest wiring cost (Figure S36).

654

655

656

659

660

661

666

667

669

670

673

674

675

676

677

678

679

682

683

684

685

686

687

688

689

691

692

693

698

699

700

701

705

706

707

708

709

710

711

Lastly, we found that an identical set of models that did not employ layer normalization typically were too unstable to train, and those that did train performed worse and exhibited weaker topography (see Figure S38 and associated text in Supporting Information). The broad but untuned effect of layer normalization thus appears to both stabilize activity and introduce a global competition that contributes to topographic organization.;

Overall, these results demonstrate the importance of sign-based constraints for developing topography in the ITN framework, and highlight that several model variants can produce topographic organization and be used for different purposes depending on the level of detail desired. More detailed analyses for these variants is available in Supporting Information (Figures S25-S32).

Networks can reduce spatial costs while maintaining performance by increasing topographic organization. The optimization problem of Equation 4 explicitly works to both maximize visual recognition performance through a task-based loss term \mathcal{L}_t , and to minimize overall wiring cost through a connectionbased lost term \mathcal{L}_w that scales with the square of connection distance. To what extent does minimizing the wiring cost term compromise performance? To answer this question, we computed wiring costs for each architecture and λ_w discussed in the previous section. We computed wiring cost in two ways. The first way is by using the \mathcal{L}_w term, which takes into account both the length and strength of connections. The second way is inspired by the wiring cost minimization framework (64), which takes into account only the length of connections, assuming sparse connectivity. To compute this wiring cost $\mathcal{L}_{w,u}$, we sparsified the network to contain only the 1% strongest connections (sparsity = 0.99), and took the averaged squared distance of remaining connections (65, see Equation 8); this sparsification introduces minimal performance deficits in the main ITN model (Figure S7). The results, shown in Figure 6D, demonstrate that increasing the wiring cost penalty λ_w by an order of magnitude decreased the first spatial cost \mathcal{L}_w by roughly an order of magnitude. Precisely, for the main architecture, the log-log plot in Figure 6D (left) revealed a power law relationship of the form $y = Ax^m$, where m = -1.24(p < 0.001). The unweighted wiring cost $L_{w,u}$ similarly decays roughly linearly on the log-log plot up to $\lambda_w = 0.1$, after which $L_{w,u}$ saturates and then rises for increasing values of λ_w . Thus, an intermediate value of λ_w appears sufficient to drive the network towards preferentially local connectivity, and further increasing λ_w may minimize further the optimization term \mathcal{L}_w through other means, such as by further shrinking small long-range weights and reducing participation at the grid boundaries where mean connection lengths are longest (see Figure S6). In contrast to the wiring costs, the final classification performance was only marginally affected by λ_w (for main model: log-log slope m = -0.0016, p < 0.001, explained variance $r^2 = 0.582$; fit was not significantly better than log-

630

631

632

633

634

637

638

639

640

641

642

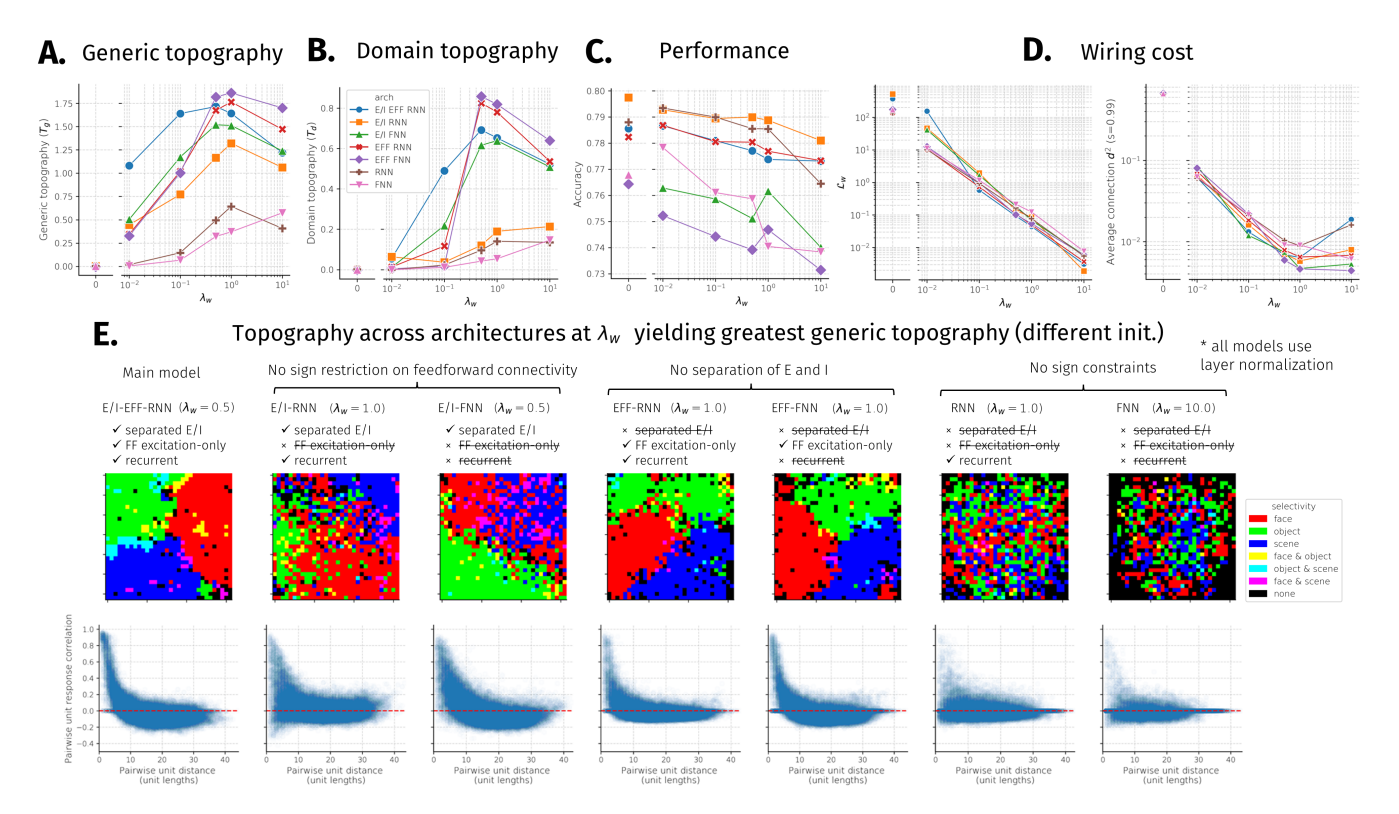


Fig. 6. Topographic organization, performance, and wiring cost as a function of spatial regularization strength (λ_w) and architectural constraints. 7 architectures were tested, sweeping all unique variations of models containing or not containing: separate excitation and inhibition (E/I), excitatory-only feedforward connectivity (EFF), and learned lateral/recurrent connections (RNN vs. FNN); see panel **D.** for a model-by-model constraint breakdown. Note that all models contained a minimal form of recurrence induced by the layer normalization operation. **A.** generic topographic organization summary statistic (Equation 7). **B.** domain-level topographic organization summary statistic (Equation 6). **C.** final accuracy on validation images. **D.** two measures of wiring cost. Left: L_w (Equation 4), right: $L_{w,u}$ (Equation 8). **E.** domain-level and generic topographic organization visualizations for each architecture using the tuned value of λ_w that maximized T_g . Each model was tested using a different random initialization from the one used to tune λ_w .

linear regression, m=-0.0028, p<0.001, explained variance $r^2=0.583$). Last, increasing the wiring cost penalty gradually resulted in the emergence of domain-selective topographic organization, along with generic topographic organization indexed by distance-dependent pairwise response correlations (see Figure 6A,B, and Figure S6). Thus, models with a large wiring cost penalty perform similarly to models with unconstrained connectivity but achieve very small wiring cost, through the development of topographic functional organization.

Discussion

714

715

716

717

718

719

720

721

722

723

724

725

726

727

728

729

730

731

732

733

734

735

736

737

738

740

Is IT cortex a collection of independent, possibly hard-wired domain-specific modules, or a more general-purpose, interactive, and plastic system? A central goal of the current work was to determine whether seemingly domain-specific organization can emerge naturally from domain-general constraints. The simulations we report demonstrate that many of the key findings thought to support a modular view of separable, innately-specified mechanisms for the recognition of different high-level domains (faces, objects, scenes) can be accounted for within a learning-based account operating under generic connectivity constraints (also see 23, 37, 76). By simulating a biologically plausible Interactive Topographic Network (ITN) model of IT without domain-specific innate structure, we found that we can "let the structure emerge" (77, 78). Specifically, we observed that the model developed largely domain-selective spatial clusters which contain preferential information for each domain, and which, when lesioned, produced largely (but not purely) specific deficits.

The equivalence of domain-general and domain-specific or**ganization.** Beyond domain-level spatially clustered organization, the model exhibited a more generic form of topographic organization, whereby nearby units had more correlated responses over images compared to more distant units, a relationship which has been demonstrated in macaque IT cortex (15, 79). In concert with other modeling work (15) that pressured neurons to obey this relationship as a proxy for wiring cost, our work suggests that this generic spatial functional relationship appears to both underly domain-level organization and emerge from wiring cost minimization. Moreover, we found that the principal components of image space were mapped across each area of model IT, as in macaque IT (14). That many of the hallmarks of domain-specificity can be simulated in a domain-general experiential account, and such domain-level organization exists within a more generic organization, gives credence to domain-general accounts that accommodate learned specialization (50, 80).

741

743

744

745

746

747

748

749

750

751

752

753

754

755

756

757

758

759

760

761

762

763

764

766

The importance of sign-based constraints alongside a minimal wiring constraint. Importantly, wiring cost and multi-task optimization (i.e., object, face, and scene image recognition), by themselves, were not sufficient to produce substantial topographic organization (Figures 6, S32). However, we found that two well-known biological details—excitatory-only betweenarea communication, and separate excitatory and inhibitory

neural populations—could induce greater topographic organization in the context of wiring cost and task optimization. Notably, locally-biased excitatory feedforward connectivity provides an inductive bias that neighboring units should have positively correlated response properties, without specifying how correlated they should be. As widespread correlation impairs representational capacity, the network is encouraged to learn in a fashion whereby pairwise correlation of neural representations decays with distance, a hallmark of topographic organization (15, 75). Models with separate excitatory and inhibitory neurons—but no restriction on which neurons sent feedforward connections—produced greater topography relative to non-sign-constrained models, but weaker topography than models with the feedforward excitation restriction. Interestingly, the feedforward E/I variant (E/I-FNN) produced stronger topographic organization than the recurrent variant (E/I RNN). Lastly, future work examining other tasks (81, 82) and architectures (83-86) that place greater functional demands on lateral connectivity may find that local connectivity constraints would make a greater contribution to topographic organization.

Comparison with other topographic algorithms. The Self-Organizing Map (SOM) (36) and other algorithms applied to early visual cortex topographic organization (28, 30) each implement a form of local cooperation alongside broader competition. Specifically, in the SOM, global competition is implemented by selecting a winning unit on each trial, and suppressing the responses of all other units, and local cooperation is mediated through Hebbian learning scaled by a Gaussian neighborhood around the winning unit. While the main ITN model is quite different from the SOM—employing error-driven rather than Hebbian learning, optimized rather than fixed lateral weights and RF sizes, hierarchical organization—one of the simple ITN variants can be seen as conceptually similar to the SOM, and this may provide insight into the minimal components of topographic development in ITN models. Specifically, we found that a feedforward model employing local excitatoryonly between-area connections and lateral connectivity limited to the layer normalization operation (EFF-FNN) was capable of producing many of the hallmarks of topographic organization in the main model (Figures 6, S31). In EFF ITN models, including this variant, the local excitatory feedforward connections (Figure 10) implement a form of local cooperation, ensuring that neighboring units are positively correlated; the layer normalization operation then implements a global competition by attempting to convert the distribution of pre-activations to a standard normal distribution, which leads to sparser activity following rectification (the degree of which can be controlled by each unit's bias term), and ensures that units represent different aspects of the feature space. Thus, layer normalization implements both competition and interactivity that, when combined with the local representational cooperation induced by local excitatory feedforward connections, leads to a smooth topographic organization whereby the unit feature tuning is systematically more similar for nearby units than for farther units. In recurrent ITN models, such as the main model, the learned lateral connections can adapt this competition and interactivity, allowing for increased performance (Figure 6C). Moreover, these learned lateral connections may contribute to competition through learned broad inhibition (Figure S17).

Despite some conceptual similarities, there are some dis-

tinct advantages to ITNs relative to SOMs and other previous topographic mapping algorithms. First, ITNs are naturally hierarchical, allowing for multiple interacting levels of topographically organized representations, rather than assuming a single feature space to be arranged in a single topographic map. This allows the ITN to account for the presence of multiple domain-selective regions arranged in a stream from earlier to later parts of IT (1, 3, 87, 88) and (in future work) to incorporate connectivity with upstream and downstream areas to IT. Second, and relatedly, the connectivity constraints of the ITN can be incorporated into generic task-optimized neural networks, without requiring separate Hebbian updates to topographically organize the feature space following development of the feature space (as in the SOM), yielding a functional rather than purely organizational role for lateral connections. Lastly, the ITN framework is very flexible, allowing for future research to examine different encoders, different IT architectures and topologies including more detailed modeling of neuronal circuitry, and different task training environments and readout mechanisms, yielding promise for a variety of future directions.

828

829

830

831

834

835

836

837

838

841

842

843

844

845

846

847

848

850

851

852

853

854

855

858

859

860

861

862

863

864

866

867

868

869

870

871

873

874

875

876

877

878

881

882

883

884

Limitations and future directions. The current work only addresses the topographic organization of high-level representations, since the connectivity constraints were not applied within the encoder model of early and mid-level vision. Modeling topographic organization in convolutional layers is a particular challenge for the ITN framework, as doing so over both retinotopic location and stimulus features—well known organizing principles of early visual cortex—would necessitate that each channel have potentially different connections with other channels across different retinotopic positions, precluding the convolution. In point of fact, feature tuning in the brain is not actually uniform across the visual field (89, 90), and thus relaxing the convolution assumption has merits for advancing visual computational neuroscience, and would enable more detailed connectivity-based topographic modeling of early and mid-level visual areas. It is now clear that convolution is not strictly required - fully connected visual "Transformer" layers using multiplicative attentional interactions (91, 92) have recently been shown to reach high performance without convolution. These architectures, and other biologically-plausible variants, thus serve as an exciting opportunity to examine topographic organization from connectivity-based constraints.

Relatedly, despite its strength in explaining hierarchical topographic organization owing to between-area spatial constraints, the ITN is not yet able to satisfactorily explain certain aspects of hierarchical representational transformationspecifically, increasing invariance to 3D rotation (14)—in contrast to the earlier convolutional layers of the encoder (Figures S13-S14). This is related to the need to use non-convolutional layers in model IT, rather than a result of the wiring or signbased constraints, as an RNN-ITN model with $\lambda = 0$ shows the same plateau of representational invariance in the ITN layers (Figure S15). Thus, our work should be seen as a demonstration that within and between-area connectivity constraints can give rise to within and between-area topographic organization, but future research will need to bridge the gap to jointly explain the increasing invariance commonly seen in standard convolutional neural networks. This again points to the critical need for future work to extend the ITN framework to more powerful computational architectures, training environments, and learning rules (93), rather than relegating this

767

768

769

770

773

774

775

777

780

781

782

783

784

785

787

789

790

791

792

793

794

797

798

799

800

801

802

803

804

805

806

807

808

810

812

813

814

815

816

817

818 819

820

821

822

823

824

computational power to a distinct encoder.

889

892

893

894

895

896

897

898

899

900

901

902

903

904

908

909

910

911

912

914

915

916

917

918

919

921

922

923

924

925

926

927

928

929

930

935

936

937

938

939

942

943

944

945

We also discovered some differences between the overarching representational space of the ITN models and primate IT. Namely, while the main ITN trained to recognize categories from 3 domains (faces, objects, and scenes) mapped these domains smoothly, the representational space elicited by a set of artificial object stimuli was less cleanly topographically organized (Figure S20A). In contrast, an alternative ITN model trained only on ImageNet (general results shown in Figures S18, S19) mapped these objects in a smoother fashion more similar to primate IT (Figure S20B) (14). However, such a model cannot account for human expertise in face recognition (Figure S18B.). Thus, each image set is limited in its ability to fully explain the empirical data. Future work employing more naturalistic datasets in which faces appear in the context of individuals in scenes alongside demands for individuation may lead to the development of representations that can more fully capture both the large-scale organization and behavioral demands of primate vision. We also found that a weaker spatial penalty resulted in less patchy topography for images outside the distribution of training images, such as the stimuli of (14) (Figure S22). Thus, a more detailed comparison of how well different ITN models quantitatively and qualitatively explain IT cortex is an exciting line for future research.

While our work advanced biological plausibility beyond previous works, by incorporating wiring constraints, the separation of excitation and inhibition, and between-area excitatory connectivity, additional biological details are likely to be important to the computation and organization of the visual cortex. Future work may seek to consider incorporating details such as E/I neuron ratio, E/I balance, variability in neuronal time constants, divisive vs. subtractive inhibitory cell types, etc. Notably, the layer normalization operation is similar to divisive normalization and its effects in activity stabilization and global untuned inhibition might be modeled in a biologically plausible fashion in future work.

Lastly, we focused on constraints local to the IT circuit, demonstrating that they can give rise to the presence of biologically realistic domain-level clusters and global generic organization. But in humans and non-human primates, domainselective regions do not merely exist, but exist in consistent locations across individuals of a given species (3, 19, 48, 94, 95), albeit with modest yet reliable individual variability (96). The retinotopic organization of upstream early visual cortical areas is thought to encourage foveally-biased cortex to support face representations, and peripherally-biased cortex to support scene representations (47, 97), and connectivity biases with downstream nonvisual areas is thought to play a further role in shaping the global organization of domain-selective areas in IT (47, 98–102). These biases, such as left-hemispheric language biases, other more fine-grained patterning of connections with domain-relevant downstream areas (i.e., sociallyresponsive areas for faces, memory areas for scenes, motor areas for manipulable objects), and cross-modal map alignment (23, 80) should be explored in future work to understand better the factors underlying IT organization both within and between hemispheres. We hypothesize that modeling longrange connectivity-based constraints with regions external to IT (e.g., 46, 47) (see also 103) in an extended ITN architecture containing two hemispheres, will give rise to reliable withinand between-hemisphere patterns of areal localization. Given that different initializations and architectural variants can yield interesting individual representational differences in deep learning models (67), we expect that a systematic study of architectural variation in ITN models could lead to successful quantitative accounting of individual differences in human cortical topography and representation.

951

952

953

954

956

957

958

959

960

961

962

963

964

965

966

968

969

970

971

972

973

974

975

976

977

978

979

980

981

982

983

984

985

986

987

988

989

990

991

992

993

994

995

996

997

998

999

1000

1001

1002

1003

1004

1005

1006

1007

1008

1009

1010

1012

1014

1016

1018

1019

1021

1022

Conclusion. The Interactive Topographic Network framework demonstrates that generic connectivity constraints can produce the central aspects of topographic organization in primate visual cortex. Extensions of the approach hold promise in accounting for the systematic localization of domain specialization both within and between hemispheres. Code will be made available upon publication at www.github.com/viscog-cmu/ITN to develop and test further ITN models.

ACKNOWLEDGMENTS. The authors thank Michael Tarr, Leila Wehbe, Vladislav Ayzenberg, Sophie Robert, Talia Konkle, Jacob Prince, and the VisCog research group at Carnegie Mellon University for helpful discussions and comments, Doris Tsao and Pinglei Bao for sharing stimuli from (14), and the three reviewers for invaluable feedback on this work. N.M.B. thanks Rosemary Cowell for early discussions that helped to conceive of the work.

References

- N Kanwisher, J McDermott, MM Chun, The Fusiform Face Area: A Module in Human Extrastriate Cortex Specialized for Face Perception. J. Neurosci. 17, 4302–4311 (1997).
- I Gauthier, et al., The fusiform "face area" is part of a network that processes faces at the individual level. J. cognitive neuroscience 12, 495–504 (2000).
- K Grill-Spector, KS Weiner, K Kay, J Gomez, The Functional Neuroanatomy of Human Face Perception. Annu. Rev. Vis. Sci. 3, 163:197 (2017).
- K Grill-Spector, T Kushnir, T Hendler, R Malach, The dynamics of object-selective activation correlate with recognition performance in humans. *Nat. Neurosci.* 3, 837–843 (2000).
- GK Aguirre, E Zarahn, M D'Esposito, An area within human ventral cortex sensitive to "Building" stimuli: Evidence and implications. Neuron 21, 373–383 (1998).
- R Epstein, N Kanwisher, A cortical representation of the local visual environment. *Nature* 392, 598–601 (1998).
- BD McCandliss, L Cohen, S Dehaene, The visual word form area: Expertise for reading in the fusiform gyrus. *Trends Cogn. Sci.* 7, 293–299 (2003).
- DY Tsao, WA Freiwald, TA Knutsen, JB Mandeville, RBH Tootell, Faces and objects in macaque cerebral cortex. Nat. Neurosci. 6, 989–995 (2003).
- DY Tsao, WA Freiwald, RBH Tootell, MS Livingstone, A Cortical Region Consisting Entirely of Face-Selective Cells. Science 311, 670–674 (2006).
- WA Freiwald, DY Tsao, Functional Compartmentalization and Viewpoint Generalization Within the Macague Face-Processing System. Science 330, 845–851 (2010).
- T Sato, et al., Object Representation in Inferior Temporal Cortex Is Organized Hierarchically in a Mosaic-Like Structure. J. Neurosci. 33, 16642–16656 (2013).
- K Tanaka, Inferotemporal Cortex and Object Vision. Annu. Rev. Neurosci. 19, 109–139 (1996).
- K Tanaka, Columns for Complex Visual Object Features in the Inferotemporal Cortex: Clustering of Cells with Similar but Slightly Different Stimulus Selectivities. Cereb. Cortex 13, 90–99 (2003).
- P Bao, L She, M Mcgill, DY Tsao, A map of object space in primate inferotemporal cortex. Nature (2020).
- H Lee, et al., Topographic deep artificial neural networks reproduce the hallmarks of the primate inferior temporal cortex face processing network, (Neuroscience), Preprint (2020).
- T Konkle, A Oliva, A Real-World Size Organization of Object Responses in Occipitotemporal Cortex. Neuron 74, 1114–1124 (2012).
- T Konkle, A Caramazza, Tripartite Organization of the Ventral Stream by Animacy and Object Size. J. Neurosci. 33, 10235–10242 (2013).
- B Long, CP Yu, T Konkle, Mid-level visual features underlie the high-level categorical organization of the ventral stream. Proc. Natl. Acad. Sci. 115, E9015–E9024 (2018).
- MJ Arcaro, MS Livingstone, A hierarchical, retinotopic proto- organization of the primate visual system at birth. eLife, 1–24 (2017).
- S Dehaene, L Cohen, J Morais, R Kolinsky, Illiterate to literate: behavioural and cerebral changes induced by reading acquisition. *Nat. Rev. Neurosci.* 16, 234–244 (2015).
- 21. M Carreiras, et al., An anatomical signature for literacy. Nature 461, 983-986 (2009)
- S Dehaene, L Cohen, Cultural Recycling of Cortical Maps. *Neuron* 56, 384–398 (2007)
- MJ Arcaro, PF Schade, MS Livingstone, Universal Mechanisms and the Development of the Face Network: What You See Is What You Get. Annu. Rev. Vis. Sci. 5, 341–372 (2019).
- BA Olshausen, DJ Field, Emergence of simple-cell receptive field properties by learning a sparse code for natural images. Nature 381, 607

 –609 (1996).
- BA Olshausen, DJ Field, Sparse coding with an overcomplete basis set: A strategy em ployed by V1? Vis. Res. 37, 3311–3325 (1997).
- DLK Yamins, et al., Performance-optimized hierarchical models predict neural responses in higher visual cortex. Proc. Natl. Acad. Sci. United States Am. 111, 8619–24 (2014).

- SM Khaligh-Razavi, N Kriegeskorte, Deep Supervised, but Not Unsupervised, Models May 1023 Explain IT Cortical Representation, PLoS Comput. Biol. 10 (2014). 1024
- C von der Malsburg, Self-organization of orientation sensitive cells in the striate cortex. Ky-1025 1026 bernetik, 85-100 (1973).
- 1027 29. R Linsker, From basic network principles to neural architecture: Emergence of orientation 1028 columns, Proc. Natl. Acad. Sci. USA, 5 (1986).

1029

1030

1031

1032

1033

1034

1035

1036

1037

1038

1039

1040

1041

1042

1043

1044

1045

1046

1047

1048

1049

1050

1051

1052

1053

1054

1055

1056

1057

1058

1059

1060

1061

1062

1063

1064

1065

1066

1067

1068

1069

1070

1071

1072

1073

1074

1075

1076

1077

1078

1079

1080

1081

1082

1083

1084

1085

1086

1087

1088

1089

1090

1091

1092

1093

1094

1095

1096

1097

1098

1099

1100

1101

1102

1106

- K Miller, J Keller, M Stryker, Ocular dominance column development; Analysis and simulation. Science 245, 605-615 (1989).
- R Durbin, G Mitchison, A dimension reduction framework for understanding cortical maps Nature 343 644-647 (1990)
- K Obermayer, H Ritter, K Schulten, A principle for the formation of the spatial structure of
- cortical feature maps. Proc. Nad. Acad. Sci. 87, 8345-8349 (1990). GJ Goodhill, DJ Willshaw, Application of the elastic net algorithm to the formation of ocular dominance stripes. Network: Comput. Neural Syst. 1, 41-59 (1990).
- GJ Goodhill, Topography and ocular dominance: A model exploring positive correlations Biol. Cybern. 69, 109-118 (1993).
- NV Swindale, The development of topography in the visual cortex: A review of models. Network: Comput. Neural Syst. 7, 161-247 (1996).
- T Kohonen, Self-organized formation of topologically correct feature maps. Biol. Cybern. 43, 59-69 (1982).
- 37 RA Cowell, GW Cottrell, What Evidence Supports Special Processing for Faces? A Cautionary Tale for fMRI Interpretation. J. Cogn. Neurosci. 25, 1777-1793 (2013).
- B Rossion, J Taubert, What can we learn about human individual face recognition from experimental studies in monkeys? Vis. Res. 157, 142-158 (2019).
- MH Tong, CA Joyce, GW Cottrell, Why is the fusiform face area recruited for novel categories of expertise? A neurocomputational investigation. Brain Res., 14-24 (2008).
- GW Cottrell, JH Hsiao, Neurocomputational Models of Face Processing. Oxf. Handb. Face Percept. (2011)
- P Grimaldi, KS Saleem, D Tsao, Anatomical Connections of the Functionally Defined "Face Patches" in the Macaque Monkey. Neuron 90, 1325-1342 (2016).
- JJ DiCarlo, D Zoccolan, NC Rust, How does the brain solve visual object recognition? Neu
- ron 73, 415-434 (2012). J Sirosh, R Miikkulainen, Topographic Receptive Fields and Patterned Lateral Interaction in
- a Self-Organizing Model of the Primary Visual Cortex. Neural Comput. 9, 577-594 (1997). R Miikkulainen, JA Bednar, Y Choe, J Sirosh, Computational Maps in the Visual Cortex.
- RA Jacobs, MI Jordan, Computational consequences of a bias toward short connections. J. Cogn. Neurosci. 4, 323-336 (1992).
- DC Plaut, Graded modality-specific specialisation in semantics: A computational account of optic aphasia. Cogn. Neuropsychol. 19, 603-639 (2002).
- DC Plaut, M Behrmann, Complementary neural representations for faces and words: A computational exploration. Cogn. Neuropsychol. 28, 251-275 (2011).
- M Behrmann, DC Plaut, Distributed circuits, not circumscribed centers, mediate visual recognition. Trends Cogn. Sci. 17, 210-219 (2013).
- M Behrmann, DC Plaut, A vision of graded hemispheric specialization. Annals New York Acad. Sci. 1359, 30-46 (2015).
- M Behrmann, DC Plaut, Hemispheric Organization for Visual Object Recognition: A Theoretical Account and Empirical Evidence. Perception 49, 373-404 (2020).
 - DLK Yamins, JJ DiCarlo, Eight open questions in the computational modeling of higher sensory cortex. Curr. Opin. Neurobiol. 37, 114-120 (2016).
 - DY Tsao, S Moeller, WA Freiwald, Comparing face patch systems in macagues and humans Proc. Natl. Acad. Sci. 14, 19514-19519 (2008)
 - DLK Yamins, JJ DiCarlo, Using goal-driven deep learning models to understand sensory cortex. Nat. Neurosci. 19, 356-365 (2016).
 - K He, X Zhang, S Ren, J Sun, Deep residual learning for image recognition, Proc. IEEE Comput. Soc. Conf. on Comput. Vis. Pattern Recognit. 2016-Decem, 770-778 (2016).
 - Q Cao, L Shen, W Xie, OM Parkhi, A Zisserman, VGGFace2: A dataset for recognising faces across pose and age in International Conference on Automatic Face and Gesture Recognition, (2018).
- J Deng, et al., ImageNet: A Large-Scale Hierarchical Image Database in CVPR. (IEEE), pp. 248-255 (2009).
 - B Zhou, A Lapedriza, A Khosla, A Oliva, A Torralba, Places: A 10 Million Image Database for Scene Recognition. IEEE Transactions on Pattern Analysis Mach. Intell. 40, 1452-1464
- NM Blauch, M Behrmann, DC Plaut, Computational insights into human perceptual expertise for familiar and unfamiliar face recognition. Cognition 208 (2021).
- HF Song, GR Yang, XJ Wang, Training Excitatory-Inhibitory Recurrent Neural Networks for Cognitive Tasks: A Simple and Flexible Framework. PLOS Comput. Biol. 12, e1004792
- JL Ba, JR Kiros, GE Hinton, Layer Normalization. arXiv:1607.06450 [cs, stat] (2016).
- B Cipollini, G Cottrell, Uniquely human developmental timing may drive cerebral lateralization and interhemispheric collaboration in Proceedings of the Cognitive Science Society, 35(35). pp. 334-339 (2013).
- N Kriegeskorte, M Mur, P Bandettini, Representational similarity analysis connecting the branches of systems neuroscience. Front. systems neuroscience 2, 4 (2008).
- G Mitchison, Neuronal branching patterns and the economy of cortical wiring. Proc. Royal Soc. London. Ser. B: Biol. Sci. 245, 151-158 (1991).
- AA Koulakov, DB Chklovskii, Orientation Preference Patterns in Mammalian Visual Cortex: A Wire Length Minimization Approach. Neuron 29, 519-527 (2001).
- D Chklovskii, Synaptic Connectivity and Neuronal MorphologyTwo Sides of the Same Coin. Neuron 43, 609-617 (2004).
- 1103 E Bullmore, O Sporns, Complex brain networks: Graph theoretical analysis of structural and 1105 functional systems. Nat. Rev. Neurosci. 10, 186-198 (2009).
 - 67. J Mehrer, CJ Spoerer, N Kriegeskorte, TC Kietzmann, Individual differences among deep

- neural network models. Nat. Commun. 11, 5725 (2020).
- JV Haxby, et al., Distributed and overlapping representations of faces and objects in ventral temporal cortex. Science 293, 2425-2430 (2001).

1107

1108

1109

1110

1111

1112

1113

1114

1115

1116

1117

1118

1119

1120

1121

1122

1123

1124

1125

1126

1127

1128

1129

1130

1131

1132

1133

1134

1135

1136

1137

1138

1139

1140

1141

1142

1143

1144

1145

1146

1147

1148

1149

1150

1151

1152

1153

1154

1155

1156

1157

1158

1159

1160

1161

1162

1163

1164

1165

1166

1167

1168

1169

1170

1171

1172

1173

1174

1175

1176

1177

1178

1179

1180

1181

1182

1183

- EM Meyers, M Borzello, WA Freiwald, D Tsao, Intelligent Information Loss; The Coding of Facial Identity, Head Pose, and Non-Face Information in the Macague Face Patch System. J. Neurosci. 35, 7069-7081 (2015).
- DE Wilson, et al., GABAergic Neurons in Ferret Visual Cortex Participate in Functionally Specific Networks. Neuron 93, 1058-1065.e4 (2017).
- DH Hubel, TN Wiesel, Anatomical Demonstration of Columns in the Monkey Striate Cortex. Nature 221 747-750 (1969)
- MJ Farah, Visual Agnosia: Disorders of Object Recognition and What They Tell Us About Normal Vision. (MIT Press), (1990).
- M Moscovitch, G Winocur, M Behrmann, What Is Special about Face Recognition? Nineteen Experiments on a Person with Visual Object Agnosia and Dyslexia but Normal Face Recognition. J. Cogn. Neurosci. 9, 555-604 (1997).
- J Geskin, M Behrmann, Congenital prosopagnosia without object agnosia? A literature review. Cogn. Neuropsychol. 3294, 1-51 (2017).
- R Kiani, H Esteky, K Mirpour, K Tanaka, Object category structure in response patterns of neuronal population in monkey inferior temporal cortex. J. Neurophysiol. 97, 4296-4309 (2007) PMID: 17428910.
- 76. K Dobs, J Martinez, AJ Kell, N Kanwisher, Brain-like functional specialization emerges spontaneously in deep neural networks, (Neuroscience), Preprint (2021).
- JL McClelland, DE Rumelhart, PR Group, , et al., Parallel Distributed Processing. (MIT press Cambridge, MA) Vol. 2, (1986).
- JL McClelland, et al., Letting structure emerge: Connectionist and dynamical systems approaches to cognition. Trends Cogn. Sci. 14, 348-356 (2010).
- NJ Majaj, H Hong, EA Solomon, JJ DiCarlo, Simple Learned Weighted Sums of Inferior Temporal Neuronal Firing Rates Accurately Predict Human Core Object Recognition Performance. J. Neurosci. 35, 13402-13418 (2015).
- MJ Arcaro, MS Livingstone, On the relationship between maps and domains in inferotemporal cortex. Nat. Rev. Neurosci. (2021).
- D Linsley, J Kim, V Veerabadran, C Windolf, T Serre, Learning long-range spatial dependencies with horizontal gated recurrent units in Advances in Neural Information Processing Systems. Vol. 2018-Decem, pp. 152-164 (2018).
- D Linsley, AK Ashok, LN Govindarajan, R Liu, T Serre, Stable and expressive recurrent vision models. arXiv:2005.11362 [cs] (2020).
- A Nayebi, et al., Task-Driven Convolutional Recurrent Models of the Visual System. arXiv, 1-14 (2018).
- J Kubilius, et al., CORnet: Modeling the Neural Mechanisms of Core Object Recognition. bioRxiv. 1-9 (2018).
- CJ Spoerer, P McClure, N Kriegeskorte, Recurrent convolutional neural networks: A better model of biological object recognition. Front. Psychol. 8, 1-14 (2017).
- CJ Spoerer, TC Kietzmann, J Mehrer, I Charest, N Kriegeskorte, Recurrent neural networks can explain flexible trading of speed and accuracy in biological vision. PLOS Comput. Biol. 16. e1008215 (2020).
- I Gauthier, P Skudlarski, JC Gore, AW Anderson, Expertise for cars and birds recruits brain areas involved in face recognition. Nat. Neurosci. 3, 191-197 (2000).
- N Kriegeskorte, E Formisano, B Sorger, R Goebel, Individual faces elicit distinct response patterns in human anterior temporal cortex. Proc. Natl. Acad. Sci. United States Am. 104, 20600-5 (2007).
- EH Silson, AWY Chan, RC Reynolds, DJ Kravitz, Cl Baker, A retinotopic basis for the division of high-level scene processing between lateral and ventral human occipitotemporal cortex. J. Neurosci. 35, 11921-11935 (2015).
- A Afraz, MV Pashkam, P Cavanagh, Spatial Heterogeneity in the Perception of Face and Form Attributes. Curr. Biol. 20, 2112-2116 (2010).
- A Vaswani, et al., Attention is all you need in Advances in Neural Information Processing Systems. Vol. 2017-Decem, pp. 5999-6009 (2017).
- 92 A Jaegle, et al., Perceiver; General perception with iterative attention (2021).
- 93. BA Richards, et al., A deep learning framework for neuroscience. Nat. Neurosci. 22, 1761-1770 (2019)
- N Kanwisher, Functional specificity in the human brain: A window into the functional architecture of the mind. Proc. Natl. Acad. Sci. United States Am. 107, 11163-11170 (2010).
- K Srihasam, JL Vincent, MS Livingstone, Novel domain formation reveals proto-architecture in inferotemporal cortex. Nat. Neurosci, 17, 1776-1783 (2014).
- M Feilong, SA Nastase, JS Guntupalli, JV Haxby, Reliable individual differences in finegrained cortical functional architecture. NeuroImage 183, 375–386 (2018). I Levy, U Hasson, G Avidan, T Hendler, R Malach, Center-periphery organization of human
- object areas. Nat. neuroscience 4, 533-539 (2001). CJ Price, JT Devlin, The interactive account of ventral occipitotemporal contributions to
- reading. Trends cognitive sciences 15, 246-253 (2011). ZM Saygin, et al., Anatomical connectivity patterns predict face selectivity in the fusiform
- gyrus. Nat. Neurosci. 15, 321-327 (2012). ZM Saygin, et al., Connectivity precedes function in the development of the visual word form
- area. Nat. Neurosci. 19, 1250-1255 (2016) BZ Mahon, A Caramazza, What drives the organization of object knowledge in the brain? Trends Cogn. Sci. 15, 97-103 (2011).
- LJ Powell, HL Kosakowski, R Saxe, Social Origins of Cortical Face Areas. Trends cognitive sciences 22, 752-763 (2018)
- HF Song, H Kennedy, XJ Wang, Spatial embedding of structural similarity in the cerebral 1185 cortex. Proc. Natl. Acad. Sci. 111, 16580-16585 (2014). 1186